Sciencexpress Report

Identification of Carbonate-Rich Outcrops on Mars by the Spirit Rover

Richard V. Morris,[1]* Steven W. Ruff,[2] Ralf Gellert,[3] Douglas W. Ming,[1] Raymond E. Arvidson,[4] Benton C. Clark,[5] D. C. Golden,[6] Kirsten Siebach,[4] Göstar Klingelhöfer,[7] Christian Schröder,[8] Iris Fleischer,[7] Albert S. Yen,[9] Steven W. Squyres[10]

[1]NASA Johnson Space Center, Houston, TX 77058, USA. [2]Arizona State University, Tempe, AZ 85287, USA. [3]University of Guelph, Guelph, Ontario, Canada. [4]Washington University in Saint Louis, St. Louis, MO 63130, USA. [5]Space Sciences Institute, Boulder, CO 80301, USA. [6]ESCG-Hamilton Sundstrand, Houston TX 77058, USA. [7]Johannes Gutenberg-Universität, Mainz, Germany. [8]University of Bayreuth and Eberhard Karls University of Tübingen, Tübingen, Germany. [9]Jet Propulsion Laboratory, Pasadena, CA 91109, USA. [10]Cornell University, Ithaca, NY 14853, USA.

*To whom correspondence should be addressed. E-mail: richard.v.morris@nasa.gov

Decades of speculation about a warmer, wetter Mars climate in the planet's first billion years call upon a denser CO_2-rich atmosphere than at present. Such an atmosphere should have led to the formation of outcrops rich in carbonate minerals, for which evidence has been sparse. Using the Mars Exploration Rover (MER) Spirit, we have now identified outcrops rich in Mg-Fe carbonate (16 to 34 wt.%) in the Columbia Hills of Gusev crater. Its composition approximates the average composition of the carbonate globules in Martian meteorite ALH 84001. The Gusev carbonate probably precipitated from carbonate-bearing solutions under hydrothermal conditions at near-neutral pH in association with volcanic activity during the Noachian era.

Carbonate minerals have long been postulated for Mars based on evidence for past and present water along with a CO_2-rich atmosphere that may have been denser during the Noachian era (*1*–*5*). They have been identified in Martian meteorites as minor phases (~1 vol.% or less) by petrographic and microbeam methods (*e.g.*, *5*) and detected from orbital observations in regional-scale rock units in Nili Fossae at unknown abundances (*6*) and, equivocally, in Martian dust and in soil as a minor component (<5 vol.%) (*7*–*10*). Here we describe the detection of carbonate as a major component in outcrops in the Columbia Hills of Gusev crater.

The Columbia Hills are an "island" of older rocks surrounded by Hesperian-aged olivine-bearing volcanic rocks that dominate the plains within Gusev crater (*11*). The Hills form a crudely antiformal structure composed of massive to layered rocks with varying compositions and extents of aqueous alteration (*12*–*16*). The Inner Basin within the Hills is dominated by volcaniclastic rocks, including Home Plate, and alteration phases (sulfates and opaline silica deposits) of likely hydrothermal origin (*17*–*21*). Spirit descended from Haskin Ridge on the eastern side of the summit of Husband Hill into the Inner Basin of the Columbia Hills to the eastern edge of the El Dorado ripple field during its second summer at Gusev crater (*16*). A series of benches (Fig. 1) with olivine-rich outcrops were encountered and analyzed by Spirit's instruments (*19*, *21*). The Comanche outcrops with their granular surface textures (grain sizes ~0.5 to 1.0 mm) are erosional remnants that are draped over the older and more massive Algonquin and other olivine- and pyroxene-rich outcrops (Figs. 1 and 2). They have layering whose bedding is roughly conformal with local topography, consistent with a volcaniclastic origin, and have fracture-filling deposits that have withstood aeolian erosion better than the surrounding materials, forming raised fins (Figs. 1 and 2).

Spirit's Mössbauer (MB) spectrometer provides information about Fe mineralogy and distribution of Fe among Fe-bearing phases and oxidation states (*22*). The Mössbauer spectrum of Comanche Spur (Fig. 3A) is characterized by two Fe^{2+} doublets, which were initially assigned to Fe^{2+} in olivine and to either Fe^{2+} in pyroxene atypical of other Gusev pyroxenes or to Fe^{2+} in a phase other than pyroxene (*19*). The doublet identification diagram (Fig. 3B), which now includes data for Fe^{2+}-bearing carbonates (*23*), shows Comanche Spur is an olivine-carbonate assemblage. The MB data indicate the presence of Mg-Fe carbonate in the Comanche outcrops [Fig. 3B and (*23*)].

In addition to major element chemistry, the Spirit's Alpha Particle X-Ray Spectrometer (APXS) instrument can determine an aggregate concentration for excess light elements through analysis of photon scattering peaks (*24*, *25*). The energy of the APXS scattering photons (14.3 keV) is virtually identical to that for the Mössbauer gamma-ray (14.4 keV), so that the depth of rock analyzed by the two instruments is equivalent. The average excess light element concentration of Comanche Spur, measured on surfaces brushed by the Rock Abrasion Tool (RAT), is 12 ± 5 wt.% equivalent CO_2 (Table 1). The low bulk CaO concentration of Comanche Spur (1.69 wt.%) requires that the carbonate have a low Ca content, consistent with Mössbauer data (Fig. 3B). For comparison, the excess light element concentration of

Algonquin is 0 ± 5 wt.% equivalent CO_2. The carbonate content of Comanche is equivalent to ~3% C in the sample. Because of CO_2 in the Martian atmosphere, this value is close to the expected APXS alpha channel detection limit for C, so we have not been able to use alpha data to detect C specifically.

We calculated the chemical composition of Comanche carbonate and olivine using previously reported APXS data (*21*), recalculated to include CO_2, and the percentages of Fe associated with those phases from MB data (Fig. 3A). The calculations yielded (Table 1) a Mg-Fe carbonate ($Mc_{0.62}Sd_{0.25}Cc_{0.11}Rh_{0.02}$ where Mc = magnesite; Sd = siderite; Cc = calcite; and Rh = rhodochrosite) and a forsteritic olivine ($Fo_{0.72}Fa_{0.28}$ where Fo = forsterite and Fa = fayalite). All Ca and Mn was assigned to the carbonate to give an upper limit concentration for those elements, but we have no information as to their actual phase association. The calculated carbonate and olivine compositions are $Mc_{0.75}Sd_{0.25}$ and $Fo_{0.70}Fa_{0.30}$ when Ca and Mn are not associated with the carbonate. In either case, the concentration of carbonate in Comanche Spur is ~26 wt.% (Table 1). Using the 7.0 to 17.0 wt.% range of the CO_2 concentration (Table 1), the range in the carbonate concentration is ~16 to 34 wt.%.

Spectra obtained by Spirit's Miniature Thermal Emission Spectrometer (Mini-TES) provide information on bulk mineralogy and modal abundance as a function of area in measured targets (*26*). Mini-TES spectra taken at eight locations on the Comanche outcrops are comparable in spectral shape (Fig. 3C), implying relatively uniform mineralogy across the outcrops. The target Taabe (Fig. 2) is on the same outcrop (Comanche Spur) as the MB and APXS targets, but the Taabe spectrum is compromised by a calibration artifact that affects the high wavenumber region (>1300 cm^{-1}; excluded in Fig. 3C) and by its cooler temperature and greater dust contribution compared to the superior spectrum obtained from target Saupitty on a different Comanche outcrop (Fig. 2).

Three absorption features attributable to fundamental infrared vibrational modes of carbonate are apparent in the Comanche Saupitty spectrum (Fig. 3D). Linear least-squares unmixing calculations (*27*) of this spectrum require carbonate to fit these features. If carbonates are excluded, the model fit is visually poorer and the root mean square error doubles (0.15% vs. 0.30%). Mg-Fe carbonate and Ca-Mg carbonate (dolomite) are spectrally indistinguishable over the wavenumber range used for the calculations. We excluded Ca-Mg carbonate from the final modeling because Ca-rich carbonates are precluded based on APXS data and are inconsistent with MB results as discussed above. Only three mineralogic components in approximately equal abundance are necessary to provide a good fit (Mg-rich olivine (Fo_{60-80}), an amorphous silicate of basaltic composition, and Mg-Fe carbonate) [Fig. 3D (*23*)].

Multispectral data obtained from the Panoramic Camera (Pancam) for the target Yackeschi (*23*) show evidence for olivine and nanophase ferric oxide, but Pancam does not cover the spectral region where the Fe^{2+} absorptions of carbonates occur (*23*).

Comanche carbonate has a well-constrained composition ($Mc_{0.62}Sd_{0.25}Cc_{0.11}Rh_{0.02}$) and is a major component based measurements made on exterior outcrop surfaces at multiple locations by both APXS and MB (~26 wt.% with a range of 16 to 34 wt.%) and Mini-TES (~34 area%). The carbonate is considered a major volumetric component rather than a surface coating because the outcrop is an erosional remnant. Martian meteorites have at most ~1 vol.% of any carbonate phase which is heterogeneously distributed and occurs as veins and fracture fills, primarily in the nakhlites (clinopyroxenites) and ALH 84001 (orthopyroxenite) (*5*, *28*, *29*). ALH 84001 has the most carbonate with an average composition [$Mc_{0.58}Sd_{0.29}Cc_{0.12}Rh_{0.01}$ (*28*, *30*)] that is similar to the Comanche carbonate composition. Synthetic analogue samples for ALH 84001 carbonate globules, with comparable average compositions ($Mc_{(0.11-0.72)}Sd_{(0.16-0.83)}Cc_{(0.06-0.17)}Rh_{(0.00-0.02)}$), have the same Mössbauer parameters as Comanche carbonate [Fig. 3B and (*23*)].

Like Comanche and ALH 84001 carbonates, orbital data for Martian dust and regional-scale surfaces in Nili Fossae point to Mg-rich carbonates, although the dust detection (<5 vol.% magnesite) has alternatively been interpreted as sulfate instead of carbonate (*7*–*9*). Visible, near-infrared (VNIR) spectra for Nili Fossae are interpreted as magnesite on the basis of two bands whose centers vary from spectrum to spectrum (2.29 to 2.31 μm and 2.49 to 2.52 μm) (*6*). Using laboratory spectra (*31*) and an assumed linear relationship in band position between $Mc_{1.00}$ and $Sd_{1.00}$, we calculated band centers at 2.31 and 2.51 μm for a Comanche-like carbonate ($Mc_{0.75}Sd_{0.25}$). Thus, Comanche and Nili Fossae carbonates have the same composition within VNIR constraints. Like Comanche carbonate, Nili Fossae carbonate is associated with olivine (*6*, *32*, *33*).

The apparently similar chemical compositions for Comanche, ALH 84001, and Nili Fossae carbonates suggest a common formation pathway. Although we do not exclude an igneous origin (*e.g.*, *34*), multiple lines of evidence point to aqueous processes under probable hydrothermal conditions. Synthetic carbonate globules with average chemical compositions similar to ALH 84001 and Comanche carbonates and Mössbauer parameters similar to the Comanche carbonate [Fig. 3B and (*23*)] were produced in the laboratory by precipitation from Mg-rich supersaturated carbonate solutions under hydrothermal conditions (~150 °C)

and near-neutral pH (~6 to 7) (*35*). Mg-rich carbonate at Spitsbergen (Norway) is interpreted to result from precipitation from hydrothermal solutions in association with volcanic activity (*36*, *37*). Morphologic (layered, clastic deposits) and mineralogic (high-SiO_2 and sulfate-rich deposits) manifestations of volcanic activity and hydrothermal processes abound in the vicinity of the Comanche outcrops, especially near Home Plate (*17–21*).

The inferred styles of hydrothermal activity at the Comanche outcrops and at Home Plate are quite different, with the former dominated by near-neutral pH, carbonate-bearing solutions [by analogy with (*35*)] and the latter dominated by acid-sulfate solutions (*18*, *19*). If the similarity in chemical composition, mineralogical composition, and association with ultramafic rock for Comanche and ALH 84001 carbonates extends to a common formation era, both carbonates are Noachian in age after ALH 84001 (*38*). In any case, Comanche outcrops on contemporary Mars may be remnants of a larger carbonate-bearing deposit that evolved in ultramafic rock in association with alkaline-neutral volcanic activity during the Noachian and then preferentially eroded (compared to massive olivine-pyroxene outcrops like Algonquin) by a combination of aeolian abrasion and chemical decomposition from exposure to acid-sulfate vapors/fluids associated with volcanic activity at Home Plate. A plausible source for carbonate-bearing solutions is, by analogy with Spitsbergen (*39*, *40*), extension of the hydrothermal system into or through subsurface carbonate-bearing rocks where carbonate dissolution took place.

The Comanche outcrops and their substantial carbonate concentration (16 – 34 wt.%) imply extensive aqueous activity under near-neutral pH conditions that would be conducive to habitable environments on early Mars. The well-separated Nili Fossae and Gusev crater carbonate locations (~6300 km on a great-circle) imply that such environments have multiple occurrences in Noachian terrain. The high carbonate concentration in the Comanche outcrops is evidence for climate models (*e.g.*, *3*) involving a CO_2 greenhouse gas on a wet and warm early Mars and subsequent sequestering of at least part of that atmosphere in carbonate minerals.

References and Notes

1. J. L. Gooding, *Icarus* **33**, 483 (1978).
2. J. L. Gooding, in *The Solar System: Observations and Interpretations, Rubey Volume IV*, M. G. Kivelson, Ed. (Prentice-Hall, 1986), pp. 208–229.
3. J. B. Pollack *et al.*, *Icarus* **71**, 203 (1987).
4. D. C. Catling, *J. Geophys. Res.* **104**, 16,453 (1999).
5. J. C. Bridges *et al.*, *Space Sci. Rev.* **96**, 365 (2001).
6. B. L. Ehlmann *et al.*, *Science* **322**, 1828 (2008).
7. J. L. Bandfield, T. D. Glotch, P. R. Christensen, *Science* **301**, 1084 (2003).
8. M. D. Lane, M. D. Dyar, J. L. Bishop, *Geophys. Res. Lett.* **31**, L19702, doi:10.1029/2004GL021231 (2004).
9. V. E. Hamilton, H. Y. McSween Jr., B. Hapke, *J. Geophys. Res.* **110**, E12006, doi:10.1029/2005JE002501 (2005).
10. W. V. Boynton *et al.*, *Science* **325**, 61 (2009).
11. M. P. Golombek *et al.*, *J. Geophys. Res.* **111**, E02S07, doi:10.1029/2005JE002503 (2006).
12. R. V. Morris *et al.*, *J. Geophys. Res.* **111**, E02S13, doi:10.1029/2005JE002584 (2006).
13. S. W. Squyres *et al.*, *J. Geophys. Res.* **111**, E02S11, doi:10.1029/2005JE002562 (2006).
14. D. W. Ming *et al.*, *J. Geophys. Res.* **111**, E02S12, doi:10.1029/2005JE002560 (2006).
15. T. J. McCoy *et al.*, *J. Geophys. Res.* **113**, E06S03, doi:10.1029/2007JE003041 (2008).
16. R. E. Arvidson *et al.*, *J. Geophys. Res.* **113**, E12S33, doi:10.1029/2008JE003183 (2008).
17. S. W. Squyres *et al.*, *Science* **316**, 738 (2007).
18. S. W. Squyres *et al.*, *Science* **320**, 1063 (2008).
19. R. V. Morris *et al.*, *J. Geophys. Res.* **113**, E12S42, doi:10.1029/2008JE003201 (2008).
20. A. S. Yen *et al.*, *J. Geophys. Res.* **113**, E06S10, doi:10.1029/2007JE002978 (2008).
21. D. W. Ming *et al.*, *J. Geophys. Res.* **113**, E12S39, doi:10.1029/2008JE003195 (2008).
22. G. Klingelhöfer *et al.*, *J. Geophys. Res.* **108**, 8067, doi:10.1029/2003JE002138 (2003).
23. Supporting material available on *Science* Online includes laboratory studies, spectral unmixing of Mini-TES spectra, and Pancam multispectral spectroscopy.
24. R. Rieder *et al.*, *J. Geophys. Res.* **108**, E12, 8066, doi:10.1029/2003JE002150 (2003).
25. J. L. Campbell *et al.*, *J. Geophys. Res.* **113**, E06S11, doi:10.1029/2007JE002959 (2008).
26. P. R. Christensen *et al.*, *J. Geophys. Res.* **108**, E12, 8064, doi:10.1029/2003JE002117 (2003).
27. M. S. Ramsey, P. R. Christensen, *J. Geophys. Res.* **103**, 577 (1998).
28. D. W. Mittlefehldt, *Meteoritics* **29,** 214 (1994).
29. A. H. Treiman, *Meteoritics* **30**, 294 (1995).
30. R. P. Harvey, H. Y. McSween Jr., *Nature* **382**, 49 (1996).
31. S. J. Gaffey, *J. Geophys. Res.* **92**, 1429 (1987).
32. T. M. Hoefen *et al.*, *Science* **302**, 627 (2003).
33. V. E. Hamilton, P. R. Christensen, *Geology* **33**, 433 (2005).
34. T. Usui, H. Y. McSween Jr., B. C. Clark III, *J. Geophys. Res.* **113**, E12S44, doi:10.1029/2008JE003225 (2008).
35. D. C. Golden *et al.*, *Meteorit. Planet. Sci.* **35**, 457 (2000).
36. A. H. Treiman *et al.*, *Earth Planet. Sci. Lett.* **204**, 323 (2002).
37. A. Steele *et al.*, *Meteorit. Planet. Sci.* **42**, 1549 (2007).
38. L. E. Borg *et al.*, *Science* **286**, 1723 (1999).

39. D. Banks *et al.*, *Geothermics* **28**, 713 (1999).
40. H. E. F. Amundsen, W. L. Griffin, S. Y. O'Reilly, *Tectonophysics* **139**, 169 (1987).
41. R.V.M. and D.W.M. acknowledge the NASA Johnson Space Center and the NASA Mars Exploration Program for support. R.V.M. acknowledges the NASA Ames Astrobiology Institute for support. S.W.R. acknowledges the NASA Mars Data Analysis Program for support. G.K. and I.F. acknowledge support by the German Space Agency DLR under contract 50QM9902. A portion of the research described in this paper was carried out at the Jet Propulsion Laboratory, California Institute of Technology, under a contract with the National Aeronautics and Space Administration. We thank P. B. Niles for carbonate samples, L. Le for carbonate microprobe analyses, and J. L. Campbell for calculation of excess light element concentrations from APXS data.

Supporting Online Material

www.sciencemag.org/cgi/content/full/science.1189667/DC1
SOM Text
Figs. S1 and S2
Tables S1 and S2
References

16 March 2010; accepted 24 May 2010
Published online 3 June 2010; 10.1126/science.1189667
Include this information when citing this paper.

Fig. 1. False color Pancam image (Sol689_P2571) looking downslope over Algonquin and Comanche outcrops. Strike and dip are indicated by black lines and arrow. Location of the Mössbauer and APXS workspace is indicated by the white circle. Inset locates from high to low elevation the olivine-rich outcrops Larry's Bench (LB), Seminole (S), Algonquin (A), and Comanche (C) on Spirit's traverse across Haskin Ridge down the southeast slope of Husband Hill. The distance between Algonquin and Comanche outcrops is ~85 m. [Image credits: NASA/JPL/Pancam and NASA/UA/HiRISE]

Fig. 2. (**A**) Navcam mosaic image of the Comanche outcrop. Taabe, Saupitty, and Yackeschi are Mini-TES and Pancam target locations. (**B**) Hazcam image that locates APXS and Mössbauer targets Horseback (H) and Palomino (P) on Comanche Spur. The objects in the lower right and left corners are rover wheels. (**C**) Pancam false-color image of the ~4.5 cm diameter RAT-brushed spots (light blue color within white circles) that shows more complete removal of surface dust for the Palomino target. MI mosaic of post-brush surfaces (field of view ~4 cm) of Comanche Spur Palomino (**D**) with a granular surface texture (grain sizes ~0.5 to 1.0 mm) and Algonquin Iroquet (**E**) with a massive surface texture. [Image credit: NASA/JPL/Navcam/Hazcam/Pancam/MI]

Fig. 3. Mössbauer spectra and Mini-TES spectra for Comanche outcrops. (**A**) Comanche Spur Mössbauer spectrum [composite of Horseback and Palomino targets (Fig. 2)]. Ol = Fe^{2+} in olivine; McSd = Fe^{2+} in Mg-Fe carbonate; npOx = Fe^{3+} in nanophase ferric oxide; and Hm = Fe^{3+} in hematite. (**B**) Mössbauer doublet identification diagram showing Gusev crater rocks and soils [after (*19*)] and terrestrial and synthetic Fe-bearing carbonates (*23*). The ranges of values of calcite (Cc) for the low- and high-Ca terrestrial and synthetic carbonates are 0.00 to 0.17 mole fraction and 0.47 to 0.95 mole fraction, respectively. The uncertainty of the subspectral area is ±2% absolute. $\delta = (v2 - v1)/2$ and $\Delta E_Q = v2 - v1$, where v1 and v2 are peak center positions numbered from low to high velocity. (**C**) Mini-TES spectra for target Taabe on Comanche Spur, target Saupitty on adjacent Comanche outcrop, and six other targets on Comanche outcrops (Fig. 2). (**D**) Model fit (blue line) for Comanche Saupitty using the three geologic phases shown (*23*). The laboratory spectrum of Mg-Fe carbonate component is shown for reference. Gray lines are one standard deviation of the 200 individual spectra averaged to produce the Saupitty spectrum.

Table 1. Chemical composition of Comanche Spur Palomino whole rock with light elements as CO_2 and calculated components olivine, carbonate, and residue.

		Component[b]		
	Whole rock[a] (wt.%)	Olivine[c] (wt.%)	Carbonate[d] (wt.%)	Residue (wt.%)
SiO_2	36.1 ± 0.4	37.8	–	62.1
TiO_2	0.22 ± 0.06	–	–	0.66
Al_2O_3	2.56 ± 0.08	–	–	7.68
Cr_2O_3	0.63 ± 0.03	–	–	1.88
Fe_2O_3	4.84 ± 0.03	–	–	14.5
FeO	15.4 ± 0.1	25.6	19.2	–
MnO	0.37 ± 0.01	–	1.43	–
MgO	21.6 ± 0.2	36.4	26.2	–
CaO	1.69 ± 0.02	–	6.55	–
Na_2O	1.0 ± 0.2	–	–	3.0
K_2O	0.03 ± 0.05	–	–	0.1
P_2O_5	0.39 ± 0.07	–	–	1.16
SO_3	2.36 ± 0.04	–	–	7.08
Cl	0.53 ± 0.01	–	–	1.61
CO_2	12 ± 5	–	46.4	–
Total	99.8	99.8	99.8	99.8
Total	99.8	40.9	25.7	33.2

[a]APXS data from (*21*) recalculated to 12 wt.% CO_2. [b]All Ca and all Mn calculated as carbonate. [c]Equivalent to $(Mg_{0.72}Fe_{0.28})SiO_4$. [d]Equivalent to $(Mg_{0.62}Fe_{0.25}Ca_{0.11}Mn_{0.02})CO_3$.

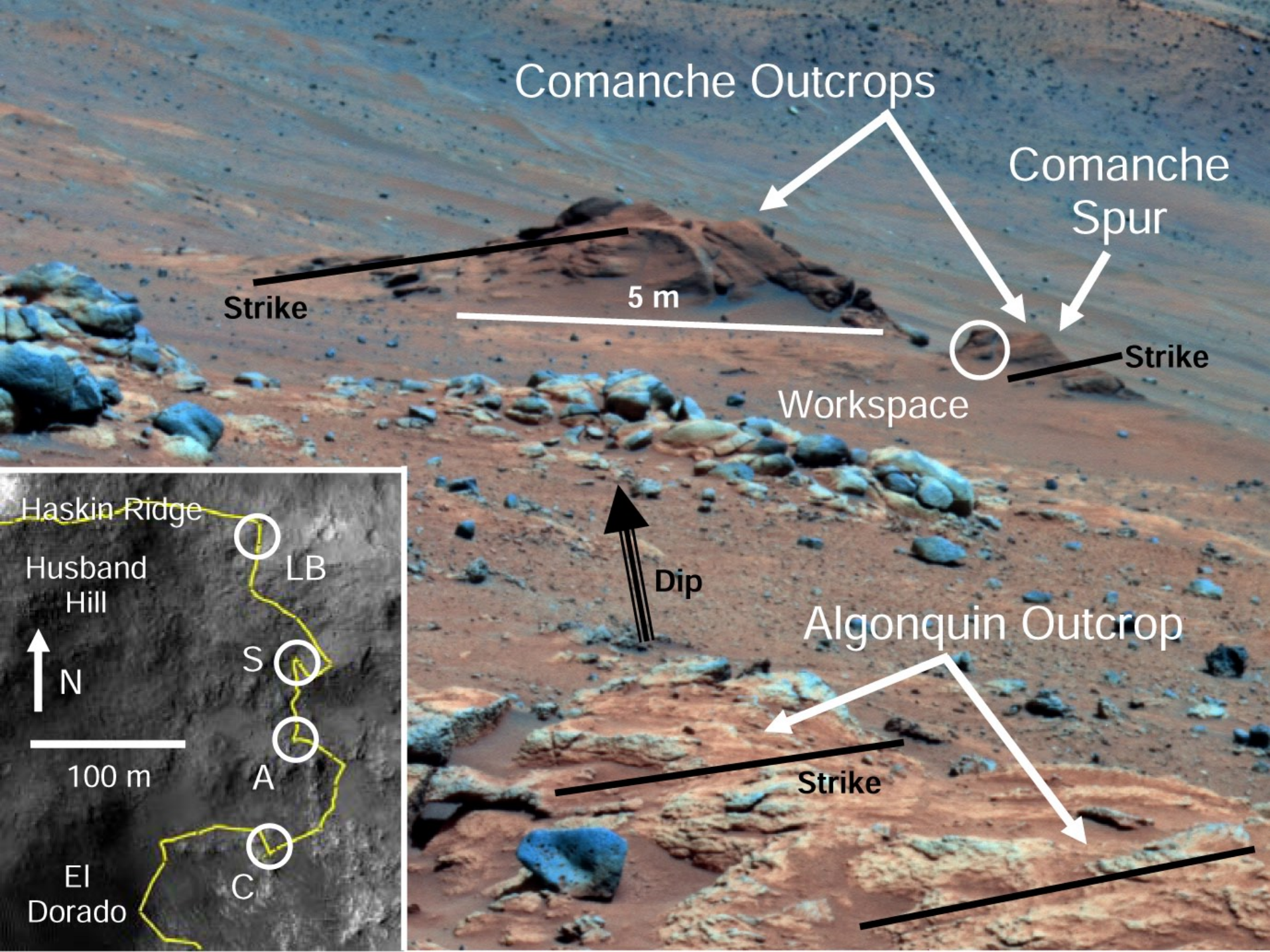
Comanche Outcrops
Comanche Spur
Strike
5 m
Strike
Workspace
Dip
Algonquin Outcrop
Strike
Haskin Ridge
Husband Hill
N
100 m
LB
S
A
C
El Dorado

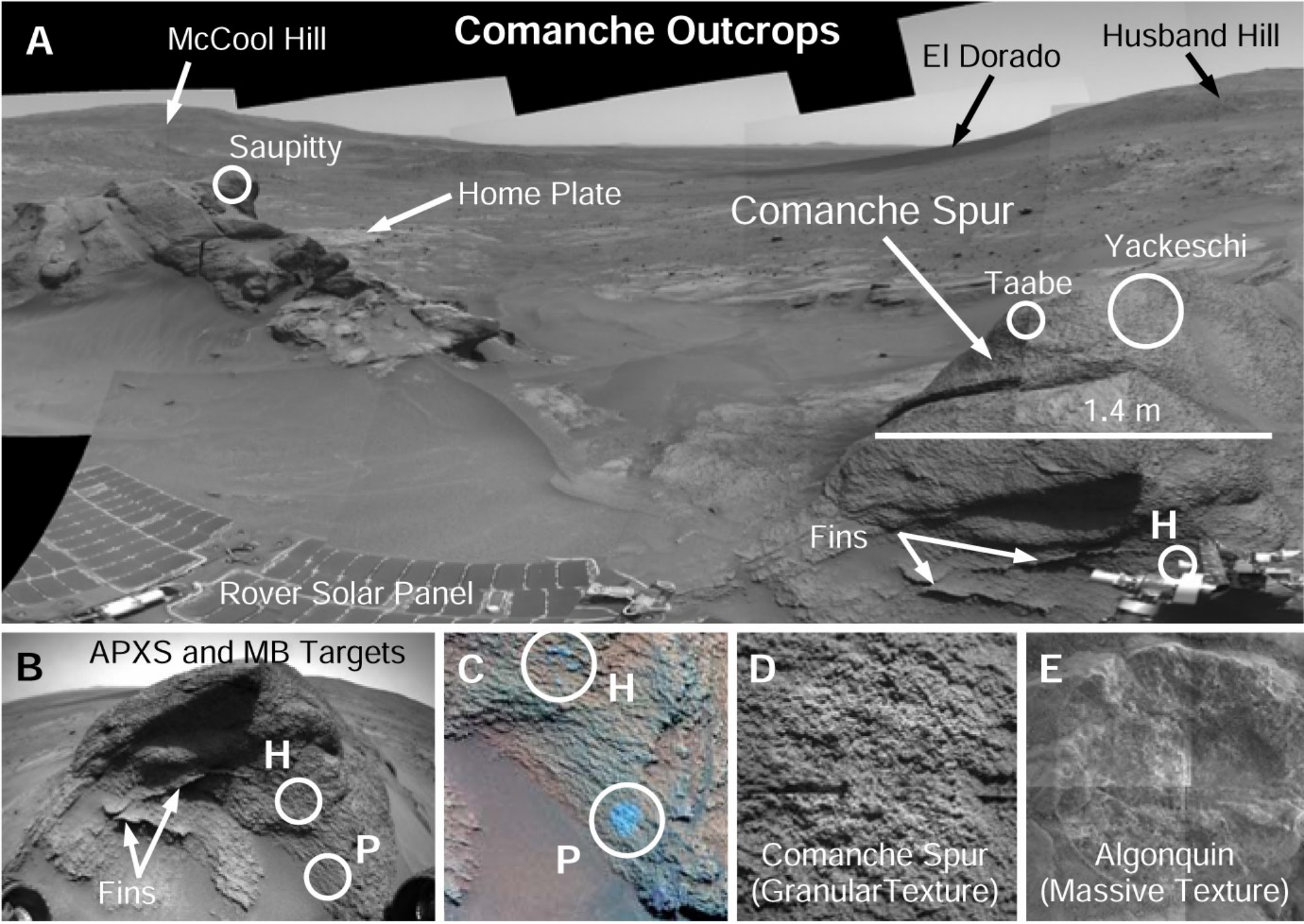
A
Comanche Outcrops
McCool Hill
El Dorado
Husband Hill
Saupitty
Home Plate
Comanche Spur
Yackeschi
Taabe
1.4 m
Fins
H
Rover Solar Panel
B
APXS and MB Targets
H
P
Fins
C
H
P
D
Comanche Spur
(GranularTexture)
E
Algonquin
(Massive Texture)

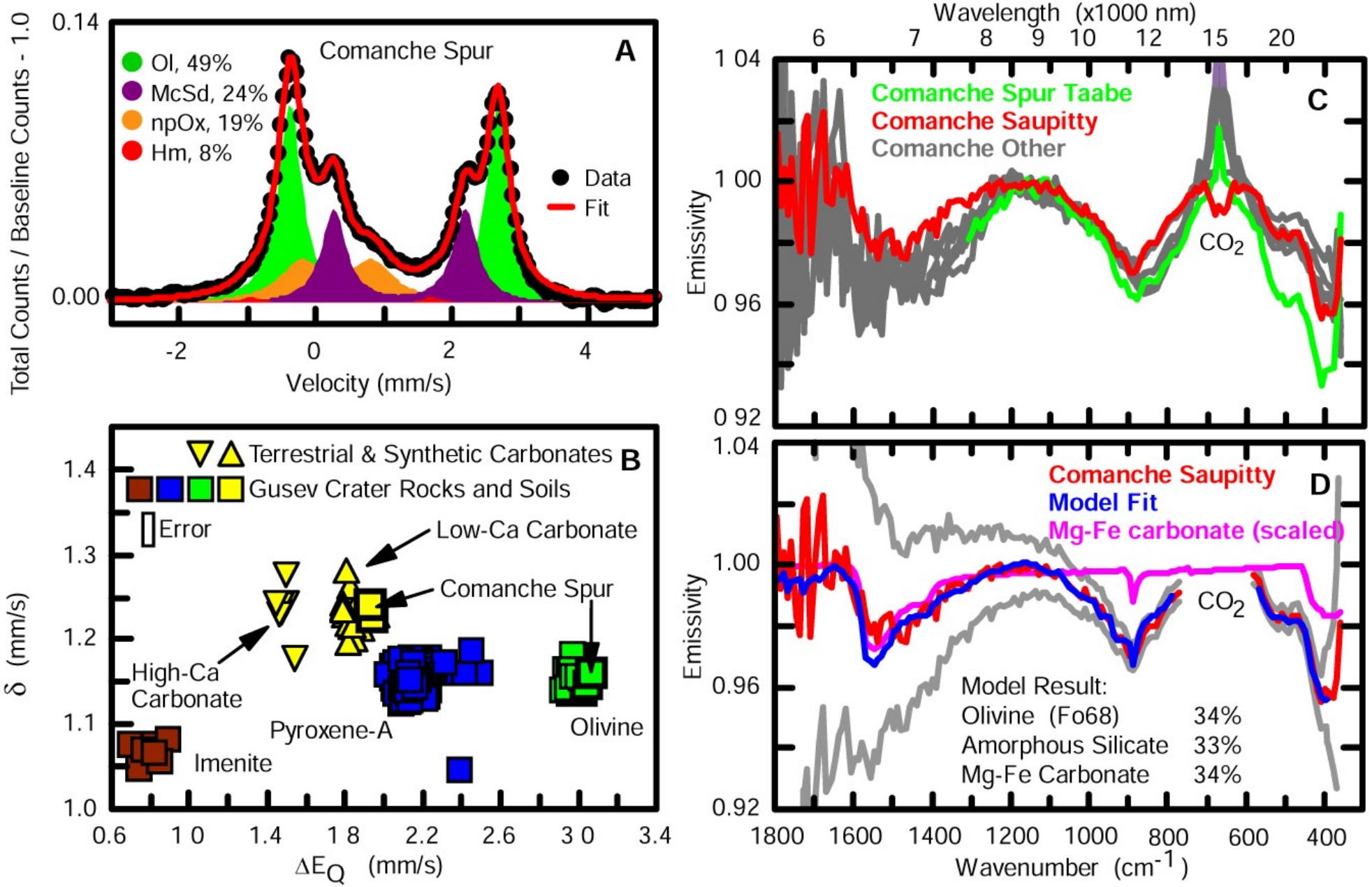
Comanche Spur
A
Ol, 49%
McSd, 24%
npOx, 19%
Hm, 8%
Data
Fit
Total Counts / Baseline Counts - 1.0
Velocity (mm/s)
Terrestrial & Synthetic Carbonates
Gusev Crater Rocks and Soils
Error
B
Low-Ca Carbonate
Comanche Spur
High-Ca Carbonate
Pyroxene-A
Olivine
Imenite
δ (mm/s)
ΔE_Q (mm/s)
Wavelength (x1000 nm)
Comanche Spur Taabe
Comanche Saupitty
Comanche Other
C
CO2
Emissivity
Comanche Saupitty
Model Fit
Mg-Fe carbonate (scaled)
D
Model Result:
Olivine (Fo68) 34%
Amorphous Silicate 33%
Mg-Fe Carbonate 34%
Wavenumber (cm-1)

Identification of Carbonate-Rich Outcrops on Mars by the Spirit Rover

Richard V. Morris, Steven W. Ruff, Ralf Gellert, Douglas W. Ming, Raymond E. Arvidson, Benton C. Clark, D. C. Golden, Kirsten Siebach, Göstar Klingelhöfer, Christian Schröder, Iris Fleischer, Albert S. Yen and Steven W. Squyres (June 3, 2010)

published online June 3, 2010

Editor's Summary

Science (print ISSN 0036-8075; online ISSN 1095-9203) is published weekly, except the last week in December, by the American Association for the Advancement of Science, 1200 New York Avenue NW, Washington, DC 20005.